

The weak magnetic field effect on dilepton polarization in heavy-ion collisions

Minghua Wei and Li Yan

*Institute of Modern Physics, Fudan University,
220 Handan Road, Shanghai 200433, China and*

*Key Laboratory of Nuclear Physics and Ion-beam Application (MOE),
Fudan University, Shanghai 200433, China*

(Dated: June 17, 2024)

Abstract

The measurement of the magnetic field created in high-energy heavy-ion collisions is challenging, due to the fact that the magnetic field decays so drastically that in a thermalized quark-gluon plasma the field strength becomes rather weak. By incorporating the weak magnetic effect into the medium, and especially into the production formalism of dileptons from the quark-gluon plasma, the effect of dilepton polarization is studied through the dilepton angular distribution. We find that the anisotropic coefficients in the dilepton spectrum are quite sensitive to the orientation and strength of the weak field. Accordingly, these coefficients provide ideal probes for the magnetic field in realistic experiments.

arXiv:2406.10041v1 [nucl-th] 14 Jun 2024

I. INTRODUCTION

A super strong electromagnetic field is created in the high-energy heavy-ion collisions. Through simple arguments from classical electrodynamics, the strength of the magnetic field is expected up to 10^{19} Gauss at the top energies at the Relativistic Heavy-Ion Collider at the Brookhaven National Laboratory [1–3]. However, experimental signatures associated with the electromagnetic field are by far rare [4–6], due to, to a large extent, the fact that the field decays so drastically that it becomes rather weak in thermalized quark-gluon plasma (QGP) [1–3, 7].

To incorporate the weak magnetic effect in a theoretical description of the QGP evolution, especially in hydrodynamical modeling which has been found extremely successful [8], a natural way is to generalize the dissipative correction by including a finite electrical current (cf. [9]). Such a current leads to effectively a weak coupling of the quarks in the QGP flow to the external electromagnetic field. As a consequence, the motion of quarks in a fluid cell is corrected according to the orientation and strength of the field, resulting in observables. In previous studies, the weak magnetic effect has been found responsible for the anisotropic emission of direct photons [10, 11], and the sign change of the local lambda hydron polarization [12].

In this study, we would like to investigate in a similar way, the weak magnetic effect on the dilepton polarization. Unlike the strong magnetic field assumption [13–18], in our analysis, the strength of the magnetic field inside QGP is treated weak, subject to the condition that $|eB| \ll m_\pi^2$, with m_π the pion mass. In high-energy heavy-ion experiments, dileptons provide a perfect electromagnetic probe for QGP. In addition to the cocktail contributions from hadron decays, heavy quarks, initial hard processes, etc., the fraction of the dilepton production from QGP thermal radiation is strongly correlated to the early-stage properties of the medium [19, 20]. The polarization of dileptons from QGP, or more precisely, the polarization of virtual photons, can be measured via the angular distribution of the dilepton spectrum [21–26]. The detailed framework of calculations will be given in Section II. With respect to the Bjorken flow solution to the QGP expansion, with a weak magnetic field whose decay is controlled by a short lifetime, we calculate the anisotropic coefficients of the dilepton angular distribution in Section III. Interestingly, the existence of a weak magnetic field leads to unambiguous signatures of the polarization properties of the dileptons, regarding their emission azimuthal angle.

II. THEORETICAL FORMULATION

A. Dilepton production rate in QGP

In a QGP medium, thermal dileptons are those produced by a virtual photon from the annihilation of a quark and an antiquark: $q\bar{q} \rightarrow \gamma^* \rightarrow l\bar{l}$. The differential production rate per volume is well known from perturbative calculations [27, 28]:

$$\frac{dR}{d^4Q} = \frac{e^4}{Q^4} \int W^{\mu\nu}(Q) L_{\mu\nu}(Q_1, Q_2) \delta^{(4)}(Q - Q_1 - Q_2) \frac{d^3\mathbf{q}_1}{(2\pi)^3 2E_1} \frac{d^3\mathbf{q}_2}{(2\pi)^3 2E_2}, \quad (2.1)$$

where Q is the four momentum of the virtual photon and it is normalized as the invariant mass, $Q^2 = M^2 > 0$. In Eq. (2.1), $L^{\mu\nu}$ is the lepton tensor. Given the momentum of the

lepton pair, q_1 and q_2 , after a summation over spins the lepton tensor can be found as¹:

$$L^{\mu\nu}(Q_1, Q_2) = -4 [(Q_1 \cdot Q_2 + m_l^2)g^{\mu\nu} - Q_1^\mu Q_2^\nu - Q_1^\nu Q_2^\mu], \quad (2.2)$$

where m_l is the mass of the lepton.

The photon tensor, $W^{\mu\nu}$, originated from the in-medium correlation of electromagnetic current. To the lowest order in the electromagnetic coupling e , but to all orders in the strong coupling constant g , $W^{\mu\nu}$ is related to the one-particle irreducible photon self-energy, $\Pi^{\mu\nu}$. The photon tensor contains the information of the QGP medium, where the dilepton is produced. In a kinetic theory approach, regardless of whether the QGP is in local thermal equilibrium, one has

$$W^{\mu\nu} = \langle w^{\mu\nu} \rangle, \quad (2.3)$$

where the angular bracket $\langle \dots \rangle$ denotes an average with respect to the quark phase-space distribution f_q and $f_{\bar{q}}$,

$$\langle A \rangle = \int \frac{d^3\mathbf{p}_1}{(2\pi)^3 2E_1} \frac{d^3\mathbf{p}_2}{(2\pi)^3 2E_2} (2\pi)^4 \delta^{(4)}(Q - P_1 - P_2) f_q f_{\bar{q}} A. \quad (2.4)$$

For a QGP in local equilibrium, the quark distribution function takes the form of the Fermi-Dirac distribution and depends explicitly on $P \cdot u/T$, with u^μ the fluid four velocity. For a QGP medium slightly out of local equilibrium due to dissipation, corrections to the distributions can be found correspondingly [11]. Especially, a weak electromagnetic field induces dissipative corrections which breaks azimuthal symmetry, irrespective of the medium expansion. For the $q\bar{q} \rightarrow l\bar{l}$ process in QGP, one also has:

$$w^{\mu\nu} = -4C_q [-(P_1 \cdot P_2 + m_q^2)g^{\mu\nu} - P_1^\mu P_2^\nu - P_2^\mu P_1^\nu] \quad (2.5)$$

where $C_q = 5/3$ is a constant factor arising from the summation over quark flavors and colors.

B. Dilepton production in terms of polarization states

Similar to the decay of a vector meson, where the polarization states of a meson can be detected in terms of the daughter particles' angular distribution [29–33], the polarization state of a virtual photon can be measured through the dilepton spectrum, especially the angular distribution [21].

As effectively a massive spin-1 particle, the polarization states of the virtual photon are captured by a spin density matrix. With respect to the polarization vector, $\varepsilon_\lambda^\mu(Q)$, with helicity $\lambda = -1, 0, +1$, the identity $\sum_\lambda \varepsilon_\lambda^\mu(Q)(\varepsilon_\lambda^\nu(Q))^* = -g^{\mu\nu} + Q^\mu Q^\nu/Q^2$ allows for a decomposition into spin states,

$$L^{\mu\nu}(Q_1, Q_2)W_{\mu\nu}(Q) = \sum_{\lambda\lambda'} (\varepsilon_\lambda^\beta)^* L_{\alpha\beta}(Q_1, Q_2) \varepsilon_{\lambda'}^\alpha (\varepsilon_{\lambda'}^\mu)^* W_{\mu\nu}(Q) \varepsilon_\lambda^\nu \equiv \sum_{\lambda, \lambda'} \rho_{\lambda, \lambda'}^{\text{lep}}(Q_1, Q_2) \rho_{\lambda', \lambda}^\gamma(Q), \quad (2.6)$$

¹ Note, however, that Eq. (2.2) corresponds to plane-wave solution which is obtained with respect to free lepton pairs. In principle, if a strong magnetic field is applied to the system, the formulation of the lepton tensor should be modified according to the correction to the motion of the lepton pairs inside the magnetic field, see Ref. [14].

where one defines,

$$\rho_{\lambda,\lambda'}^{\text{lep}}(Q_1, Q_2) \equiv (\varepsilon_\lambda^\beta)^* L_{\alpha\beta}(Q_1, Q_2) \varepsilon_{\lambda'}^\alpha \quad \text{and} \quad \rho_{\lambda,\lambda'}^\gamma(Q) \equiv (\varepsilon_{\lambda'}^\mu)^* W_{\mu\nu}(Q) \varepsilon_\lambda^\nu, \quad (2.7)$$

as the spin density matrices of the lepton pair and the virtual photon, respectively. Note that the decomposition is achieved owing to the vector current conservation, which guarantees $Q_\mu L^{\mu\nu} = Q_\mu W^{\mu\nu} = 0$, and $Q_\mu \varepsilon_\lambda^\mu(Q) = 0$.

With respect to the helicity $\lambda = \pm 1$ and 0 , $\varepsilon_\lambda^\mu(Q)$ indicates the eigenstate of a massive virtual photon with transversal polarizations and longitudinal polarization, respectively. Correspondingly, as the current-current correlator being decomposed into the spin states², the spin density matrix of the virtual photon, ρ^γ , contains information on polarization of the intermediate state during the di-lepton production. Because statistical factors arise due to the thermal nature of the QGP medium, as well as the average over initial and final states during quark-antiquark annihilation, the density matrix ρ^γ captures a mixed state, so that $\text{tr}(\rho^\gamma)^2 < \text{tr}\rho^\gamma \equiv \rho_{-1,-1}^\gamma + \rho_{0,0}^\gamma + \rho_{+1,+1}^\gamma$. Here, the trace is taken in the spin subspace. By construction, the spin density matrix is hermitian. Therefore, upon a normalization factor which will be shown proportional to the dilepton production rate, and the hermiticity condition, the virtual photon spin density matrix ρ^γ contains five independent components.

The differential production rate of a dilepton pair from QGP can be described in terms of the polarization states of the virtual photon. In particular, one notices that the dilepton production rate is proportional to the trace of the virtual photon spin density matrix. This can be shown through integration with respect to the relative momentum $Q' = Q_1 - Q_2$ in Eq. (2.6), which leads to $\int d^4Q' \rho_{\lambda,\lambda'}^{\text{lep}} \propto \int d^4Q' \varepsilon_\lambda^\alpha(Q) [Q^2 g_{\alpha\beta} - Q_\alpha Q_\beta + Q'_\alpha Q'_\beta] \varepsilon_{\lambda'}^\beta(Q) \propto \delta_{\lambda,\lambda'}$, and correspondingly,

$$\frac{dR}{d^4Q} = \frac{\alpha_{\text{EM}}^2}{3\pi^3 M^2} \left(1 + \frac{2m_l^2}{M^2} \right) \sqrt{1 - \frac{4m_l^2}{M^2}} \text{tr}\rho^\gamma. \quad (2.8)$$

Eq. (2.8) implies that the two transversal and one longitudinal polarization states of the virtual photon contribute equally to the production of the dilepton pair, which can be understood, for instance, in an eigen system that diagonalizes the density matrix.

All the individual components in the virtual photon density matrix are involved in the angular distribution of the dilepton pair. Unlike the rate, the angular distribution of the produced dileptons is not Lorentz invariant. For convenience, one chooses the virtual photon rest frame with $Q = (M, \mathbf{0})$ and $Q' = (0, \mathbf{q}') = (0, 2\mathbf{q}_1)$, where $|\mathbf{q}_1| = |\mathbf{q}_2| = \sqrt{\frac{M^2}{4} - m_l^2}$ is the magnitude of the 3-momentum of the lepton in the virtual photon rest frame. Accordingly, given a specified quantization axis, one is allowed to parameterize the lepton four-momentum in terms of the solid angle $\Omega_l = (\theta_l, \phi_l)$,

$$Q_1^\mu = \left(\sqrt{m_l^2 + \mathbf{q}_1^2}, |\mathbf{q}_1| \sin \theta_\ell \cos \phi_\ell, |\mathbf{q}_1| \sin \theta_\ell \sin \phi_\ell, |\mathbf{q}_1| \cos \theta_\ell \right), \quad (2.9a)$$

$$Q_2^\mu = \left(\sqrt{m_l^2 + \mathbf{q}_1^2}, -|\mathbf{q}_1| \sin \theta_\ell \cos \phi_\ell, -|\mathbf{q}_1| \sin \theta_\ell \sin \phi_\ell, -|\mathbf{q}_1| \cos \theta_\ell \right). \quad (2.9b)$$

² Note that the current-current correlator $W^{\mu\nu}$ characterizes an intermediate vector state, namely, the virtual photon, inside a QGP medium.

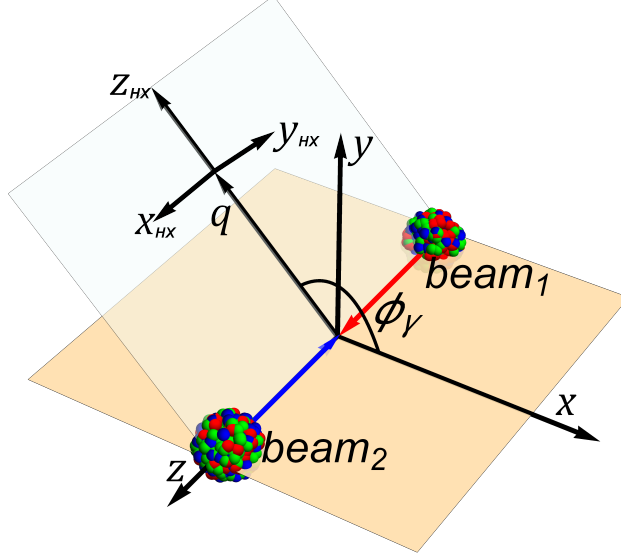


FIG. 1. Coordinate configuration in the helicity frame. As the quantization axis (Z_{HX} -axis) is given by the three momentum of the virtual photon, \mathbf{q} , the production plane is then determined by Z_{HX} and the beam axis (z -axis), which accordingly determines X_{HX} . And ϕ_γ is the angle between the virtual photon and the reaction plane

Substituting Eqs. (2.9) into Eq. (2.2) yields an expression of $L^{\mu\nu}$ in terms of θ_ℓ and ϕ_ℓ [23], and accordingly leads to [34–36],

$$\frac{dR}{d^4Q d\Omega_\ell} = \frac{\alpha_{\text{EM}}^2}{16\pi^4 M^2} \left(1 - \frac{4m_l^2}{M^2}\right)^{3/2} \mathcal{N} (1 + \lambda_\theta \cos^2 \theta_\ell + \lambda_\phi \sin^2 \theta_\ell \cos 2\phi_\ell + \lambda_\phi^\perp \sin^2 \theta_\ell \sin 2\phi_\ell + \lambda_{\theta\phi} \sin 2\theta_\ell \cos \phi_\ell + \lambda_{\theta\phi}^\perp \sin 2\theta_\ell \sin \phi_\ell), \quad (2.10)$$

where $\mathcal{N} = (1 + 2m_l^2/|\mathbf{q}_1|^2)\text{tr}\rho^\gamma + \rho_{0,0}^\gamma$ is the normalization factor. These five independent anisotropic coefficients λ_θ , λ_ϕ , $\lambda_{\theta\phi}$, λ_ϕ^\perp and $\lambda_{\theta\phi}^\perp$, are defined through the components of the spin density matrix of the virtual photon. For instance,

$$\lambda_\theta = \frac{1}{\mathcal{N}}(\rho_{-,-}^\gamma + \rho_{+,+}^\gamma - 2\rho_{0,0}^\gamma), \quad \lambda_\phi = \frac{2}{\mathcal{N}}\text{Re}\rho_{+,-}^\gamma, \quad \lambda_{\theta\phi} = \frac{\sqrt{2}}{\mathcal{N}}\text{Re}(\rho_{+,0}^\gamma - \rho_{-,0}^\gamma). \quad (2.11)$$

Several comments are in order. First, in the dilepton angular distribution, the six independent angular modes (including the constant term) in Eq. (2.10) are originated from the $Q'_\alpha Q'_\beta$ factor in the lepton tensor. In the local rest frame of the virtual photon, for instance, the factor reduces to the direct product of three-vectors, $q'_i q'_j$, which can be decomposed into six independent irreducible tensors with respect to the $\text{SO}(3)$ symmetry group. In fact, the independent number of angular modes should be identical in arbitrary frames, owing to the transversality condition $Q \cdot Q' = 0$.³ Secondly, even in the virtual photon rest frame, these anisotropic coefficients depend on the specification of a quantization axis. Throughout this work, we choose the so-call helicity frame (HX), in which the quantization axis follows

³ For the electromagnetic decay of a virtual photon, this transversality condition is a consequence of the conservation of lepton number. However, for the weak decay process of a vector meson, the transversality condition is not available and hence one expects more angular modes in the angular distribution of final state particles.

the direction of the three momentum of the virtual photon, $\hat{z}_{\text{HX}} = \hat{q}$. A production plane, which consists of the beam axis in experiments (z -axis) and the quantization axis, can be determined accordingly. The helicity frame is feasible in realistic experiments, as long as the three momentum of generated dilepton pairs is identified. The configuration of the helicity frame coordinates is depicted in Fig. 1. For later convenience, we also choose in the helicity frame the polarization vectors (circular polarization) as,

$$\begin{aligned}\epsilon^\mu(-1) &= \frac{1}{\sqrt{2}}(0, 1, -i, 0), \\ \epsilon^\mu(0) &= (0, 0, 0, 1), \\ \epsilon^\mu(+1) &= -\frac{1}{\sqrt{2}}(0, 1, i, 0).\end{aligned}\tag{2.12}$$

Thirdly, these coefficients reveal the nature of virtual photon polarization. For instance, in the limit $m_l \rightarrow 0$, one notices that λ_θ reduces to,

$$\lambda_\theta = \frac{\rho_{-,-}^\gamma + \rho_{+,+}^\gamma - 2\rho_{0,0}^\gamma}{\rho_{-,-}^\gamma + \rho_{+,+}^\gamma + 2\rho_{0,0}^\gamma} \in [-1, 1],$$

where the lower bound (-1) is realized with respect to a longitudinally polarized virtual photon with $\rho_{\pm,\pm}^\gamma = 0$, and the upper bound ($+1$) corresponds to a transversely polarized virtual photon with $\rho_{0,0}^\gamma = 0$. For an unpolarized virtual photon, namely, $\rho_{-,-}^\gamma = \rho_{+,+}^\gamma = \rho_{0,0}^\gamma$, λ_θ vanishes. The angular modes involving ϕ_ℓ break azimuthal symmetry in the virtual photon rest frame, reflecting the mixing among polarization states of the virtual photon.

C. Polarization states of a virtual photon inside a weak magnetic field

Being generated from the in-medium Drell-Yan process, the polarization states of a virtual photon depend strongly on the motion of quarks. In a static medium, for instance, where the quarks are distributed in phase space isotropically, in the rest frame of the virtual photon a longitudinal polarization could be induced owing to the Lorentz boosted flow velocity $U^\mu = \gamma(1, -\vec{v}_{\gamma*})$ [21, 24]. Moreover, an even polarized state should be expected in the medium in the presence of an extra vector that breaks the rotational symmetry. For instance, a finite electromagnetic field in the fluid local rest frame gives rise to the electric field, $E^\mu = F^{\mu\nu}U_\nu$, where $F^{\mu\nu}$ is the electromagnetic field strength tensor.

In the case of a weak magnetic field, the hydrodynamic description of QGP contains dissipative correction associated with the conserved electric charge. In terms of the net electric charge flow, it is $\Delta j^\mu = \sigma_{\text{el}}E^\mu$, where σ_{el} is the electrical conductivity of the QGP. In a kinetic theory approach, correspondingly, the dissipative correction to quark local equilibrium distribution can be solved. To the leading order of $|eB|/T^2$, one finds for quark species $a = u, d, s$ and $\bar{u}, \bar{d}, \bar{s}$, with electric charge number Q_a [11],

$$\delta f_{\text{EM}}^{(a)}(X, \mathbf{p}) = \frac{n_{\text{eq}}(1 + n_{\text{eq}})}{P \cdot U} \frac{\sigma_{\text{el}}}{T\chi_{\text{el}}} eQ_a F^{\mu\nu} P_\mu U_\nu,\tag{2.13}$$

where χ_{el} is an effective charge susceptibility of the QGP system. Note that in Eq. (2.13) the spin degrees of freedom of individual quarks have been averaged. More detailed information regarding Eq. (2.13) can be found in [11]. In the current study, we shall ignore the dissipative

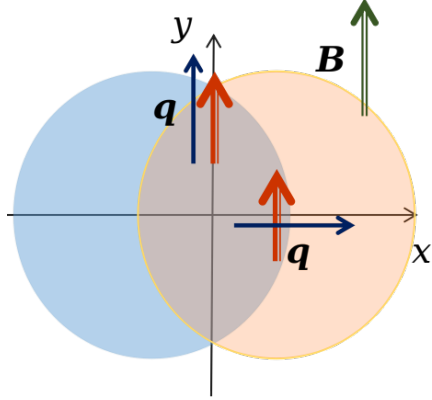


FIG. 2. (Color online) Thermal virtual photon polarization (red arrows) is induced aligned (or anti-aligned, not shown) with the external magnetic field (green arrow) in heavy-ion collisions. Correspondingly, the emitted virtual photons along the x -axis are expected to be transversely polarized, while the virtual photons emitted out of the reaction plane are expected to be longitudinally polarized.

correction due to viscosities, so that the in-medium average of the virtual photon polarization tensor is given by an integral in Eq. (2.4), with $f_q = n_{\text{eq}} + \delta f_{\text{EM}}$.

In the lab frame, as the QGP being created by the colliding nuclei, a finite electromagnetic field is also generated by the relativistic motion of spectators, especially in non-central collisions⁴. Up to fluctuations, the induced electromagnetic field is dominated by its magnetic component, orientated out of the reaction plane, namely, $\mathbf{B} = B_y \hat{y}$. Accordingly, Eq. (2.13) implies that the dissipative contribution to virtual photons via the weak external magnetic field involves quarks with a finite velocity in the reaction plane (x - z plane). Since the quark spin has been averaged, as the quark-antiquark pair annihilates, the polarization states of the produced virtual photons are related to the quarks' orbital angular momentum, which is aligned or anti-aligned with the magnetic field. Therefore, as demonstrated in Fig. 2, in the presence of a weak external magnetic field, in the lab frame the virtual photons are polarized along the magnetic field. Correspondingly, the virtual photons emitted along the x -axis are transversely polarized, while the virtual photons emitted out of reaction are longitudinally polarized.

III. DILEPTON POLARIZATION FROM THE BJORKEN FLOW

As shown in Eq. (2.13), the coupling of the weak magnetic field to QGP requires a finite flow velocity. To this end, we consider, for the simplest case, the Bjorken flow, which has a longitudinal expansion.

Bjorken flow gives rise to an analytical description of the 1+1 dimensional expanding QGP,⁵ subject to the Bjorken boost symmetry along the longitudinal direction determined by the collision axis, and the translational invariance in the transverse plane. It is believed that Bjorken flow approximates the early-stage evolution of QGP in high-energy heavy-ion

⁴ Even in ultra-central collisions, on an event-by-event basis, the external electromagnetic field presents with a random orientation, although the field is expected to vanish over the event average.

⁵ Bjorken flow is actually 0+1 dimensional since the dependence on space-time rapidity in the Milne coordinates is suppressed.

collisions, during which the medium expansion is dominated in the longitudinal direction until a time scale that is comparable to the system size. On the other hand, one also notices that owing to the temperature dependence of the dilepton production rate, there are more thermal dileptons generated during the early times of the QGP evolution, which makes our calculation more reliable with respect to the realistic high-energy heavy-ion collisions.

In the Milne coordinates, where the proper time and the space-time rapidity are introduced respectively as,

$$\tau = \sqrt{t^2 - z^2}, \quad \xi = \tanh^{-1} \left(\frac{z}{t} \right), \quad (3.1)$$

the flow four velocity in Bjorken flow is well determined, $u^\mu = (1, 0, 0, 0)$, and the medium evolution depends only on τ . For instance, as we shall consider for simplicity in our calculation, the evolution of temperature in an ideal fluid is given as

$$T(\tau) = T(\tau_0) \left(\frac{\tau_0}{\tau} \right)^{1/3}. \quad (3.2)$$

This information suffices to allow one to evaluate Eq. (2.13) and to calculate the production of the thermal dileptons. We thus follow all the procedures introduced in the previous sections, and focus on the electron-positron pair production, with electron mass $m_e = 0.51$ MeV. For quarks in the QGP medium, our analysis includes up and down quarks and their anti-particles, with their masses $m_u = m_d = m_q = 5$ MeV.

In high-energy heavy-ion collisions, the external magnetic field decays as the QGP medium expands. Due to the lack of knowledge of the electrical conductivity in QGP, however, the exact space-time dependence of the magnetic field remains undetermined so far. In this work, we consider a magnetic field that distributes homogeneously in space in the lab frame, while its time dependence is given by [7, 37, 38],

$$B(\tau) = \frac{B_0}{1 + (\tau/\tau_B)^2}. \quad (3.3)$$

In the above equation, B_0 corresponds to the field strength at the instant of the nucleus-nucleus collision, and the parameter τ_B is used to characterize the lifetime of the magnetic field. With respect to the mid-central Au-Au collisions with $\sqrt{s_{\text{NN}}} = 200$ MeV at RHIC, we take $eB_0 = 3m_\pi^2$ [2, 3]. The lifetime of the magnetic field is to a large extent determined by the appearance of a Lorentz factor in the relativistic collisions, and a small enhancement due to the finite electrical conductivity in the medium [7, 39, 40]. Nonetheless, at the top RHIC energies, the lifetime of the magnetic field is expected no longer than 1 fm/c. In this work, we shall allow τ_B to increase from 0.2 fm/c, to 0.4 fm/c and 0.6 fm/c, correspondingly, the effect of the field on the QGP evolution gets stronger.

The medium properties of QGP are determined by the solution of the ideal Bjorken flow. We take $T(\tau_0) = 300$ MeV at $\tau_0 = 1.0$ fm/c, and sum up the produced dileptons down to $\tau_f = 5$ fm/c. We choose a temperate dependent electrical conductivity, with its value extracted from perturbative quantum chromodynamics calculation, $\sigma_{\text{el}}/T = 2$ [41].

For convenience, we do not distinguish the difference between the center-of-momentum frame and the lab frame. In the lab frame, the momentum of the virtual photon can be expressed by:

$$(Q^\mu)_{\text{Lab}} = (M_T \cosh y, q_T \cos \phi_\gamma, q_T \sin \phi_\gamma, M_T \sinh y) \quad (3.4)$$

where $M_T = \sqrt{q_T^2 + M^2}$ is the transverse mass and q_T is the transverse momentum of dilepton. ϕ_γ is the angle between the dilepton(virtual photon) and the reaction plane, and y

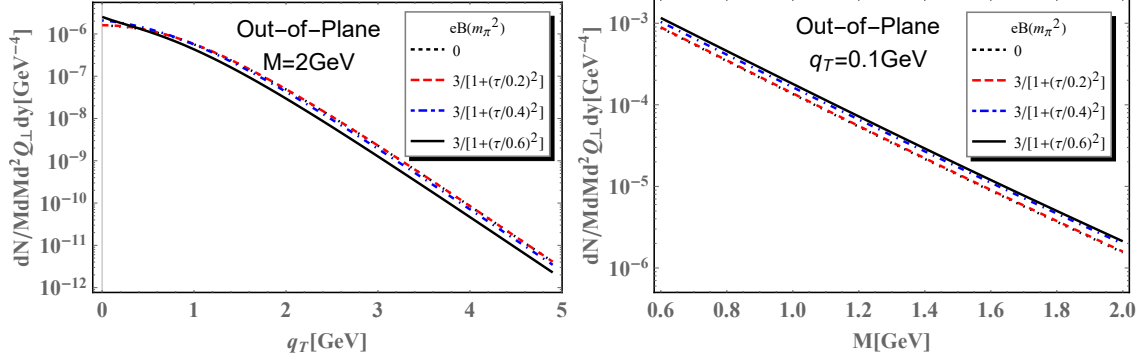


FIG. 3. (Color online) The production rate of the electron-positron pair as a function of the virtual photon transverse momentum q_T (left) and invariant mass M (right). The rapidity is fixed at $y = 0$. The black dotted lines stand for zero magnetic field case. The red dashed, blue dot-dashed, and black solid lines stand for finite magnetic fields with lifetime $\tau_B = 0.2, 0.4, 0.6$ fm/c, respectively.

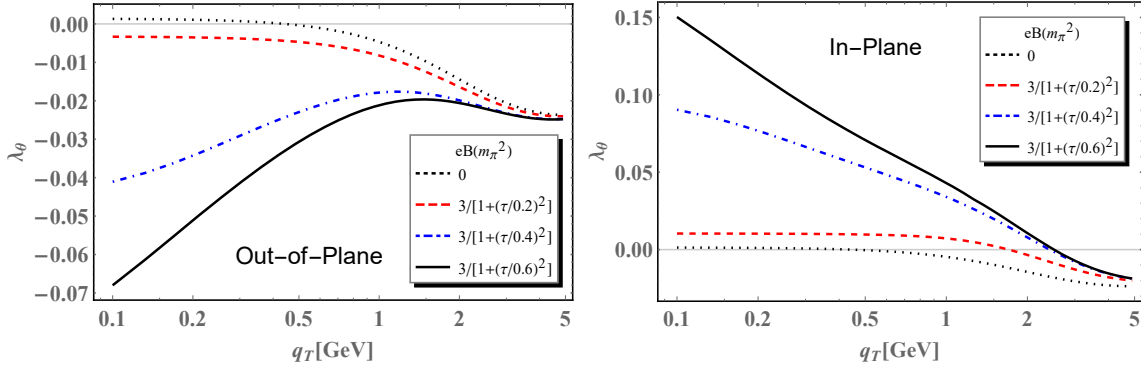


FIG. 4. λ_θ as a function of transverse momentum q_T from QGP with Bjorken expansion. The black dotted lines stand for zero magnetic field case. The red dashed, blue dot-dashed, and black solid lines stand for finite magnetic fields with lifetime $\tau_B = 0.2, 0.4, 0.6$ fm/c, respectively.

is the rapidity. We also use the $Q_\perp = (q_T \cos \phi_\gamma, q_T \sin \phi_\gamma)$ to make the following expressions compact.

In Fig. 3, the differential production rate of the thermal dilepton in QGP is shown as a function of the transverse momentum of the virtual photon q_T with fixed virtual photon invariant mass $M = 2$ GeV (left panel), and a function of the virtual photon invariant mass M with $q_T = 0.1$ GeV (right panel). In comparison to the case of pure QGP evolution (black dotted lines), the weak external magnetic field leads to small corrections to the dilepton spectrum.

With respect to the dilepton polarization, on the other hand, the effect of the weak magnetic field is remarkable, as shown through the anisotropic coefficient λ_θ in Fig. 4. Here, we take the invariant mass as $M = 2$ GeV, at which the dominant non-cocktail contribution to the dilepton spectrum is from QGP [42]. In previous studies [24], it has been noticed that, due to the Lorentz boost, even for a QGP with Bjorken expansion, the produced dileptons are polarized with a finite λ_θ . Such an effect is reproduced and shown as the black dotted lines in Fig. 4. Because the background QGP medium is azimuthally symmetric, without the external magnetic field, the resulted dilepton polarization is azimuthally symmetric as

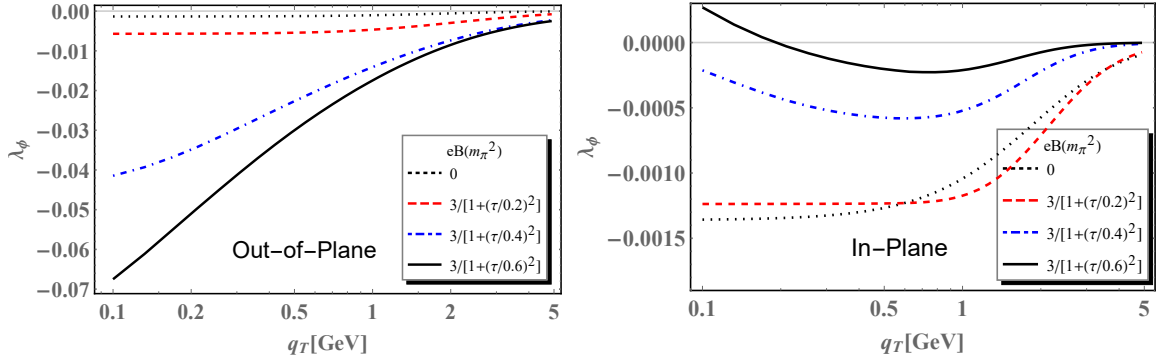


FIG. 5. λ_ϕ as a function of transverse momentum q_T in a Bjorken flow. The black dotted lines stand for zero magnetic field case. The red dashed, blue dot-dashed, and black solid lines stand for finite magnetic fields with lifetime $\tau_B = 0.2, 0.4, 0.6$ fm/c, respectively.

well with respect to the emission angle of the dilepton, ϕ_γ (cf. Fig. 1). In the presence of a weak external magnetic field, the polarization in the produced dilepton gets enhanced significantly. Moreover, the polarization of the dilepton reflects apparent azimuthal angle dependence. In the small q_T region, where the effect of the magnetic field overwhelms the effect of Lorentz boost, one observes longitudinal polarization for the out-of-plane dileptons ($\phi_\gamma = \pi/2$), and transverse polarization for the in-plane dileptons ($\phi_\gamma = 0$), in consistency with our previous analysis in Section II C. In the large q_T region, the polarization in the dilepton is dominated by the Lorentz boost, hence the dependence on the magnetic field becomes negligible.

Regarding the dileptons with invariant mass $M = 2$ GeV, we also calculated λ_ϕ , with results shown in Fig. 5. Because the coefficient λ_ϕ characterizes the polarization in the azimuthal direction with respect to the virtual photon momentum, the effect from the Lorentz boost is marginal. However, in the presence of the weak external magnetic field along the y -axis, Bjorken flow implies the coupling of the magnetic field to quarks moving in the reaction plane, namely, $B_y u_z p_x$. As a consequence, for the di-lepton pairs produced along the x -axis, or in plane, azimuthal symmetry with respect to the virtual photon three momentum is barely broken, and the induced λ_ϕ is small. On the other hand, for the di-leptons emitted out of the reaction plane, the azimuthal symmetry with respect to the three momentum is apparently broken, one accordingly gets a finite and negative λ_ϕ , as shown in the figures.

IV. SUMMARY AND DISCUSSION

In this work, we analyzed the polarization property of thermal dileptons from QGP. Especially, we found that an external magnetic field in the QGP medium, albeit weak, could induce a significant effect on the polarization of the produced dileptons. Quite similar to the direct photon production and lambda hyperon polarization [11, 12], the weak magnetic effect in QGP, has a small correction to the transverse momentum and invariant mass dependence of the dilepton spectrum. However, as the motion of quark and anti-quark pairs get extra alignment associated with the orientation of the magnetic field, the resulting change in the dilepton angular distribution can be remarkable.

Using the ideal Bjorken flow to describe the QGP expansion, we calculated the anisotropic coefficients in the dilepton spectrum. Although the calculation is simplified, for instance,

medium expansion in the transverse directions and anisotropic flow of the QGP are neglected, to a large extent, we believe our results are reliable. First, as we mentioned previously, the emission of dileptons from QGP is dominated in the early stages, where the medium expansion is mainly one dimensional. Secondly, at the early stages, the anisotropic flow of the QGP is not substantial, its influence to the dilepton production is expected small.

Our results indicate that the anisotropic coefficients in the dilepton spectrum, λ_θ and λ_ϕ are both observables sensitive to the external magnetic field. For the low p_T emission and invariant mass $M = 2$ GeV, these coefficients reach up to 10^{-1} , which we expect to be measurable at the RHIC collisions within errors. In particular, the dependence on the emission angle provides a qualitative probe to identify the existence of the magnetic field in relativistic heavy-ion collisions. As a major result of the current study, we propose that a finite and positive λ_θ , and a negligible λ_ϕ , for the dileptons emitted in the reaction plane, together with the finite and negative λ_θ and λ_ϕ for the dileptons emitted out of the reaction plane, as the unambiguous signature of the effect of the external magnetic field.

ACKNOWLEDGMENTS

We would like to thank Qiye Shou for the very helpful discussion that motivated our study. We wish to acknowledge the support of the Natural Science Foundation of Shanghai (No. 23JC1400200). This work is also supported partly by the National Natural Science Foundation of China (NSFC No. 12375133 and No. 12147101).

-
- [1] Dmitri E. Kharzeev, Larry D. McLerran, and Harmen J. Warringa, “The Effects of topological charge change in heavy ion collisions: ‘Event by event P and CP violation’,” *Nucl. Phys. A* **803**, 227–253 (2008), [arXiv:0711.0950 \[hep-ph\]](#).
 - [2] V. Skokov, A. Yu. Illarionov, and V. Toneev, “Estimate of the magnetic field strength in heavy-ion collisions,” *Int. J. Mod. Phys. A* **24**, 5925–5932 (2009), [arXiv:0907.1396 \[nucl-th\]](#).
 - [3] Wei-Tian Deng and Xu-Guang Huang, “Event-by-event generation of electromagnetic fields in heavy-ion collisions,” *Phys. Rev. C* **85**, 044907 (2012), [arXiv:1201.5108 \[nucl-th\]](#).
 - [4] Berndt Müller and Andreas Schäfer, “Chiral magnetic effect and an experimental bound on the late time magnetic field strength,” *Phys. Rev. D* **98**, 071902 (2018), [arXiv:1806.10907 \[hep-ph\]](#).
 - [5] M. I. Abdulhamid EMet al. (STAR), “Global polarization of Λ and Λ^- hyperons in Au+Au collisions at sNN=19.6 and 27 GeV,” *Phys. Rev. C* **108**, 014910 (2023), [arXiv:2305.08705 \[nucl-ex\]](#).
 - [6] M. I. Abdulhamid EMet al. (STAR), “Observation of the electromagnetic field effect via charge-dependent directed flow in heavy-ion collisions at the Relativistic Heavy Ion Collider,” *Phys. Rev. X* **14**, 011028 (2024), [arXiv:2304.03430 \[nucl-ex\]](#).
 - [7] Anping Huang, Duan She, Shuzhe Shi, Mei Huang, and Jinfeng Liao, “Dynamical magnetic fields in heavy-ion collisions,” *Phys. Rev. C* **107**, 034901 (2023), [arXiv:2212.08579 \[hep-ph\]](#).
 - [8] Chun Shen and Li Yan, “Recent development of hydrodynamic modeling in heavy-ion collisions,” *Nucl. Sci. Tech.* **31**, 122 (2020), [arXiv:2010.12377 \[nucl-th\]](#).
 - [9] S. R. De Groot, *EMRelativistic Kinetic Theory. Principles and Applications*, edited by W. A. Van Leeuwen and C. G. Van Weert (1980).

- [10] Jing-An Sun and Li Yan, “The effect of weak magnetic photon emission from quark-gluon plasma,” (2023), [arXiv:2302.07696 \[nucl-th\]](#).
- [11] Jing-An Sun and Li Yan, “Estimating the magnetic field strength in heavy-ion collisions via direct photon elliptic flow,” *Phys. Rev. C* **109**, 034917 (2024), [arXiv:2311.03929 \[nucl-th\]](#).
- [12] Jing-An Sun and Li Yan, “Weak magnetic effect in quark-gluon plasma and local spin polarization,” (2024), [arXiv:2401.07458 \[nucl-th\]](#).
- [13] Kirill Tuchin, “Magnetic contribution to dilepton production in heavy-ion collisions,” *Phys. Rev. C* **88**, 024910 (2013), [arXiv:1305.0545 \[nucl-th\]](#).
- [14] N. Sadooghi and F. Taghinavaz, “Dilepton production rate in a hot and magnetized quark-gluon plasma,” *Annals Phys.* **376**, 218–253 (2017), [arXiv:1601.04887 \[hep-ph\]](#).
- [15] Aritra Das, Najmul Haque, Munshi G. Mustafa, and Pradip K. Roy, “Hard dilepton production from a weakly magnetized hot QCD medium,” *Phys. Rev. D* **99**, 094022 (2019), [arXiv:1903.03528 \[hep-ph\]](#).
- [16] Xinyang Wang, Igor A. Shovkovy, Lang Yu, and Mei Huang, “Ellipticity of photon emission from strongly magnetized hot QCD plasma,” *Phys. Rev. D* **102**, 076010 (2020), [arXiv:2006.16254 \[hep-ph\]](#).
- [17] Nilanjan Chaudhuri, Snigdha Ghosh, Sourav Sarkar, and Pradip Roy, “Dilepton production from magnetized quark matter with an anomalous magnetic moment of the quarks using a three-flavor PNJL model,” *Phys. Rev. D* **103**, 096021 (2021), [arXiv:2104.11425 \[hep-ph\]](#).
- [18] Xinyang Wang and Igor A. Shovkovy, “Rate and ellipticity of dilepton production in a magnetized quark-gluon plasma,” *Phys. Rev. D* **106**, 036014 (2022), [arXiv:2205.00276 \[nucl-th\]](#).
- [19] Julien Serreau, “Out-of-equilibrium electromagnetic radiation,” *JHEP* **05**, 078 (2004), [arXiv:hep-ph/0310051](#).
- [20] H. T. Ding, A. Francis, O. Kaczmarek, F. Karsch, E. Laermann, and W. Soeldner, “Thermal dilepton rate and electrical conductivity: An analysis of vector current correlation functions in quenched lattice QCD,” *Phys. Rev. D* **83**, 034504 (2011), [arXiv:1012.4963 \[hep-lat\]](#).
- [21] R. Arnaldi EMet al. (NA60), “First results on angular distributions of thermal dileptons in nuclear collisions,” *Phys. Rev. Lett.* **102**, 222301 (2009), [arXiv:0812.3100 \[nucl-ex\]](#).
- [22] G. Agakishiev EMet al. (HADES), “Dielectron production in Ar+KCl collisions at 1.76A GeV,” *Phys. Rev. C* **84**, 014902 (2011), [arXiv:1103.0876 \[nucl-ex\]](#).
- [23] Enrico Speranza, Miklós Zétényi, and Bengt Friman, “Polarization and dilepton anisotropy in pion-nucleon collisions,” *Phys. Lett. B* **764**, 282–288 (2017), [arXiv:1605.04954 \[hep-ph\]](#).
- [24] Enrico Speranza, Amaresh Jaiswal, and Bengt Friman, “Virtual photon polarization and dilepton anisotropy in relativistic nucleus–nucleus collisions,” *Phys. Lett. B* **782**, 395–400 (2018), [arXiv:1802.02479 \[hep-ph\]](#).
- [25] Florian Seck, Bengt Friman, Tetyana Galatyuk, Hendrik van Hees, Enrico Speranza, Ralf Rapp, and Jochen Wambach, “Polarization of Thermal Dilepton Radiation,” (2023), [arXiv:2309.03189 \[nucl-th\]](#).
- [26] Maurice Coquet, Xiaojian Du, Jean-Yves Ollitrault, Soeren Schlichting, and Michael Winn, “Dilepton polarization as a signature of plasma anisotropy,” (2023), [arXiv:2309.00555 \[nucl-th\]](#).
- [27] Larry D. McLerran and T. Toimela, “Photon and Dilepton Emission from the Quark - Gluon Plasma: Some General Considerations,” *Phys. Rev. D* **31**, 545 (1985).
- [28] H. A. Weldon, “Reformulation of finite temperature dilepton production,” *Phys. Rev. D* **42**, 2384–2387 (1990).
- [29] Zuo-Tang Liang and Xin-Nian Wang, “Spin alignment of vector mesons in non-central A+A

- collisions,” *Phys. Lett. B* **629**, 20–26 (2005), [arXiv:nucl-th/0411101](#).
- [30] Shreyasi Acharya EMet al. (ALICE), “First measurement of quarkonium polarization in nuclear collisions at the LHC,” *Phys. Lett. B* **815**, 136146 (2021), [arXiv:2005.11128 \[nucl-ex\]](#).
- [31] M. S. Abdallah EMet al. (STAR), “Pattern of global spin alignment of ϕ and K^{*0} mesons in heavy-ion collisions,” *Nature* **614**, 244–248 (2023), [arXiv:2204.02302 \[hep-ph\]](#).
- [32] Yan-Qing Zhao, Xin-Li Sheng, Si-Wen Li, and Defu Hou, “Holographic spin alignment of J/ψ meson in magnetized plasma,” (2024), [arXiv:2403.07468 \[hep-ph\]](#).
- [33] Xin-Li Sheng, Yan-Qing Zhao, Si-Wen Li, Francesco Becattini, and Defu Hou, “Holographic spin alignment for vector mesons,” (2024), [arXiv:2403.07522 \[hep-ph\]](#).
- [34] K. Gottfried and John David Jackson, “On the Connection between production mechanism and decay of resonances at high-energies,” *Nuovo Cim.* **33**, 309–330 (1964).
- [35] K. Schilling, P. Seyboth, and Guenter E. Wolf, “On the Analysis of Vector Meson Production by Polarized Photons,” *Nucl. Phys. B* **15**, 397–412 (1970), [Erratum: *Nucl.Phys.B* 18, 332 (1970)].
- [36] Pietro Faccioli, Carlos Lourenco, Joao Seixas, and Hermine K. Wohri, “Model-independent constraints on the shape parameters of dilepton angular distributions,” *Phys. Rev. D* **83**, 056008 (2011), [arXiv:1102.3946 \[hep-ph\]](#).
- [37] Shuzhe Shi, Yin Jiang, Elias Lilleskov, and Jinfeng Liao, “Anomalous Chiral Transport in Heavy Ion Collisions from Anomalous-Viscous Fluid Dynamics,” *Annals Phys.* **394**, 50–72 (2018), [arXiv:1711.02496 \[nucl-th\]](#).
- [38] Kun Xu, Shuzhe Shi, Hui Zhang, Defu Hou, Jinfeng Liao, and Mei Huang, “Extracting the magnitude of magnetic field at freeze-out in heavy-ion collisions,” *Phys. Lett. B* **809**, 135706 (2020), [arXiv:2004.05362 \[hep-ph\]](#).
- [39] Gabriele Inghirami, Luca Del Zanna, Andrea Beraudo, Mohsen Haddadi Moghaddam, Francesco Becattini, and Marcus Bleicher, “Numerical magneto-hydrodynamics for relativistic nuclear collisions,” *Eur. Phys. J. C* **76**, 659 (2016), [arXiv:1609.03042 \[hep-ph\]](#).
- [40] Li Yan and Xu-Guang Huang, “Dynamical evolution of a magnetic field in the preequilibrium quark-gluon plasma,” *Phys. Rev. D* **107**, 094028 (2023), [arXiv:2104.00831 \[nucl-th\]](#).
- [41] Peter Brockway Arnold, Guy D Moore, and Laurence G. Yaffe, “Transport coefficients in high temperature gauge theories. 2. Beyond leading log,” *JHEP* **05**, 051 (2003), [arXiv:hep-ph/0302165](#).
- [42] A. Adare EMet al. (PHENIX), “Dielectron production in Au+Au collisions at $\sqrt{s_{NN}}=200$ GeV,” *Phys. Rev. C* **93**, 014904 (2016), [arXiv:1509.04667 \[nucl-ex\]](#).